2017

Kepler observations of the pulsating subdwarf B star KIC 2697388: the detection of converging frequency multiplets in the full data set

J. W. Kern
MSU Undergraduate

Michael D. Reed
Missouri State University

A. S. Baran

R. H. Østensen
Missouri State University

J. H. Telting

Recommended Citation

Kern, J. W., M. D. Reed, A. S. Baran, R. H. Østensen, and J. H. Telting. "Kepler observations of the pulsating subdwarf B star KIC 2697388: The detection of converging frequency multiplets in the full data set." Monthly Notices of the Royal Astronomical Society (2017).

Monthly Notices
of the
ROYAL ASTRONOMICAL SOCIETY

MNRAS **465,** 1057–1065 (2017)
Advance Access publication 2016 November 2

doi:10.1093/mnras/stw2794

Kepler observations of the pulsating subdwarf B star KIC 2697388: the detection of converging frequency multiplets in the full data set

J. W. Kern,[1] M. D. Reed,[1]★ A. S. Baran,[2] R. H. Østensen[1] and J. H. Telting[3]

[1]*Department of Physics, Astronomy and Materials Science, Missouri State University, 901 S. National, Springfield, MO 65897, USA*
[2]*Suhora Observatory and Krakow Pedagogical University, ul. Podchorąży ch 2, PL-30-084 Kraków, Poland*
[3]*Nordic Optical Telescope, Rambla José Ana Fernández Pérez 7, E-38711 Breña Baja, Spain*

Accepted 2016 October 26. Received 2016 October 21; in original form 2016 August 12

ABSTRACT

The *Kepler* spacecraft observed ∼150 000 stars over the course of its four-year mission, of which 18 were discovered to be pulsating subdwarf B stars, including KIC 2697388. We analyse three years of *Kepler* spacecraft short-cadence data as well as 21 low-resolution spectra of the pulsating subdwarf B star KIC 2697388. Our spectra have a radial-velocity scatter of 9.5 km s^{-1}, and while insufficient to completely rule out binarity, we rule out short-period, low-inclination orbits for KIC 2697388. From the short-cadence *Kepler* data, we detect 253 periodicities, most with periods from 1 to 2.5 h, which we associate with gravity-mode pulsations. Twenty-three periods were also detected in the short-period pressure-mode region. We applied standard seismic tools for mode identification, including asymptotic overtone period spacings and rotationally induced frequency multiplets. We classify 89 per cent of the periodicities with mode identifications; most of low degree ($\ell \leq 2$), but 42 are identified as $\ell \geq 3$. Frequency multiplets provide a rotation period for the star of ∼42 d. A unique feature is seen in KIC 2697388's data; in all $\ell \geq 2$ multiplets, the splittings decrease over the course of the observations. If the trend continues, $\ell \geq 2$ multiplets would become singlets within a decade.

Key words: stars: oscillations.

1 INTRODUCTION

Subdwarf B (sdB) stars are extreme horizontal branch stars and have, on average, core masses of ∼0.5 solar masses, radii of 0.2 solar radii, and effective temperatures of ∼30 000 K (Heber et al. 1984; Saffer et al. 1994). Two classes of sdB variables are known: short-period pulsators, with periods under ∼15 min associated with pressure (p-) modes, and long-period pulsators, with periods from 0.75 to 8 h associated with gravity (g-) modes. Reviews of sdB stars and their pulsation properties include Østensen (2010, ground-based) and Reed & Foster (2014, including *Kepler* discoveries).

The *Kepler* spacecraft was launched in 2009 and has accumulated a unique data set. Never before, and with no current plans for future missions, have stars been observed at a rapid cadence (1 min) continuously for multiple years. Such a data set has greatly advanced our knowledge of stellar structure and evolution via the application of asteroseismology. For sdB stars, these data have allowed, for the first time, bulk observational constraints of pulsation modes, which are a requirement for the application of asteroseismology. A total of 18 pulsating sdB stars were discovered during the four-year *Kepler* mission, most of which were observed in short-cadence mode (SC; 58.86 s integrations) for over three years with a duty cycle above 90 per cent. Of these stars, 2 are predominantly p-mode pulsators, 15 are predominantly g-mode pulsators, and 1 has many of each type (Østensen et al. 2010, 2011; Baran et al. 2012; Østensen et al. 2014). To date, only six of these stars have had their full *Kepler* data sets analysed and published (Østensen et al. 2014; Reed et al. 2014; Telting et al. 2014; Baran et al. 2015, 2016; Foster et al. 2015). Seismic milestones include the discovery of evenly spaced asymptotic overtones in period (Reed et al. 2011), some with a few trapped modes (Østensen et al. 2014), and frequency multiplets with splittings which vary as predicted by the Ledoux formula (Baran et al. 2012). Asymptotic overtone sequences can be used to identify pulsation modes and discern structural boundaries (Reed et al. 2011); frequency multiplets also provide mode identifications, bulk and internal rotation rates, and constraints on the pulsation axis. These tools have been used to discern stochastic, time-dependent amplitudes (Østensen et al. 2014), subsynchronously rotating binaries (Pablo et al. 2012), and a pulsator where the core rotates nearly three times slower than the surface (Foster et al. 2015).

KIC 2697388 was discovered to be a pulsator from one month of SC observations (Q2.3; the third month of the second quarter)

★ E-mail: mikereed@missouristate.edu

during *Kepler's* first year of operation, which was largely a survey year (Østensen et al. 2010). Østensen et al. (2010) also did a spectral analysis which resulted in $T_{\rm eff} = 23900 \pm 300$ K, $\log(g) = 5.32 \pm 0.03$ dex, and $\log(N_{\rm He}/N_{\rm H}) = -2.9 \pm 0.1$ dex. From the Q2.3 data, Reed et al. (2010) found KIC 2697388 to be a hybrid pulsator. They detected 1 p-mode pulsation and 36 g-mode periodicities. Charpinet et al. (2011) also analysed the Q2.3 data set, listing 59 frequencies, and performed a seismic model fitting using their third-generation models. The best-fitting model had $T_{\rm eff} = 25395 \pm 227$ K, $\log(g) = 5.500 \pm 0.031$dex, and $\log(N_{\rm He}/N_{\rm H}) = -2.767 \pm 0.122$ dex, in good agreement with measurements of Østensen et al. (2010). Using the first nine months of continuous *Kepler* SC observations for KIC 2697388 (quarters 5, 6, and 7), Baran (2012) detected 148 periodicities, including asymptotic period spacings of 240.06 ± 0.46 and 138.80 ± 0.19 s for $\ell = 1$ and 2 modes, respectively. They also detected frequency multiplets and calculated a rotation period of 45.55 ± 4.75 d. In total, they associated 89 (60 per cent) of their periodicities as $\ell = 1$ (2) modes.

In this paper, we examine the entire *Kepler* SC data set for KIC 2697388, as well as spectroscopic observations taken using the Nordic Optical Telescope (NOT) and William Herschel Telescope (WHT).

2 SPECTROSCOPY

As part of our programme obtaining follow-up spectroscopy of *Kepler*-observed pulsators, low-resolution spectra ($R \approx 2000$–2500) have been collected using the 2.56-m NOT with ALFOSC, grism #16 and a 0.5 arcsec slit, and the 4.2-m WHT with ISIS, the R600B grating and 1.0 arcsec slit. The resulting resolutions based on the width of arc lines are 1.7 and 2.2 Å for the setups at the WHT and NOT, respectively. Exposure times were between 500 and 900 s. The 3 WHT spectra were obtained on the nights of 2010 July 27 and 28, and the 18 NOT spectra on 10 nights throughout 2011 May–July. The signal-to-noise ratio (S/N) of the WHT spectra ranges from 87 to 114; the S/N of the NOT spectra ranges between 33 and 63.

After applying standard reduction steps, including correction to the heliocentric frame, we used a cross-correlation technique to look for possible orbital radial-velocity (RV) variability. While the RV measurements show considerable scatter with rms = 9.5 km s^{-1}, we could not find any significant periodic RV signal. The RV data are consistent with KIC 2697388 being a single star but are not of sufficient accuracy to rule out binarity.

We used the average spectrum for each telescope, both with S/N ~ 190, to get a first estimate of the basic atmospheric parameters based on high-S/N spectral data. For this purpose, we used the fitting procedure of Edelmann et al. (2003), with the metal-line blanketed local thermodynamic equilibrium (LTE) models of solar composition described in Heber, Reid & Werner (2000). For the WHT spectrum, we get $T_{\rm eff} = 24\,262 \pm 86$ K, $\log(g) = 5.34 \pm 0.011$ dex, and $\log(N_{\rm He}/N_{\rm H}) = -2.9128 \pm 0.0224$ dex. For the NOT spectrum, we find $T_{\rm eff} = 23\,390 \pm 118$ K, $\log(g) = 5.29 \pm 0.015$ dex, and $\log(N_{\rm He}/N_{\rm H}) = -2.9111 \pm 0.020\,90$ dex. A fit to the lines is shown in Fig. 1.

3 DATA PROCESSING AND ANALYSES

We processed and analysed the SC *Kepler* data in a similar fashion to our previous papers (e.g. Reed et al. 2014) and summarized as follows: We downloaded optimally extracted light curves from the Mikulski Archive for Space Telescopes,[1] used low-order spline fitting to remove long-term trends (>1.5 d), and normalized the data with the mean brightness. We sigma-clipped the data at 5σ and multiplied the modulation intensities so amplitudes would appear in a Fourier transform (FT) as parts per thousand (ppt). The full SC data set spans 1147.5 d and includes 1.54 million individual observations (a 91.4 per cent duty cycle), which is a $1.5/T$ temporal resolution of 0.0159 μHz. There are about 0.8 million resolved frequencies up to the Nyquist, requiring a detection threshold of 4.8σ to ensure that any random peak is unlikely due to noise. We calculate this amplitude detection threshold to be 0.431 ppt using regions of the frequency spectrum free from pulsations. Periodicities with amplitudes close to this level are considered provisional, unless secondary evidence (such as asymptotic period spacing or frequency splittings) is found. Previous analyses of full *Kepler* data sets have often revealed variability in pulsation amplitudes and/or frequencies. Therefore, we examined data over several different time-scales, to best determine which pulsations are likely intrinsic to the star. We produced FTs of the entire data set (sample region shown in Fig. 2), the data set in halves, and three-quarter (nine month) sets stepped by a quarter. We also created sliding FTs (sFTs) to see how these frequencies evolve with time. Sliding FTs were made using data spanning 200 d and stepping them by 5 d over the entire data set. The FTs are then stacked into one resultant graph which plots frequency versus time, where the amplitude of each pulsation is indicated by the colour scale, given in sigma (example shown in Fig. 3). Where peaks in the full-length FT were higher than the detection limit, we visually inspected the sFT and the other FTs

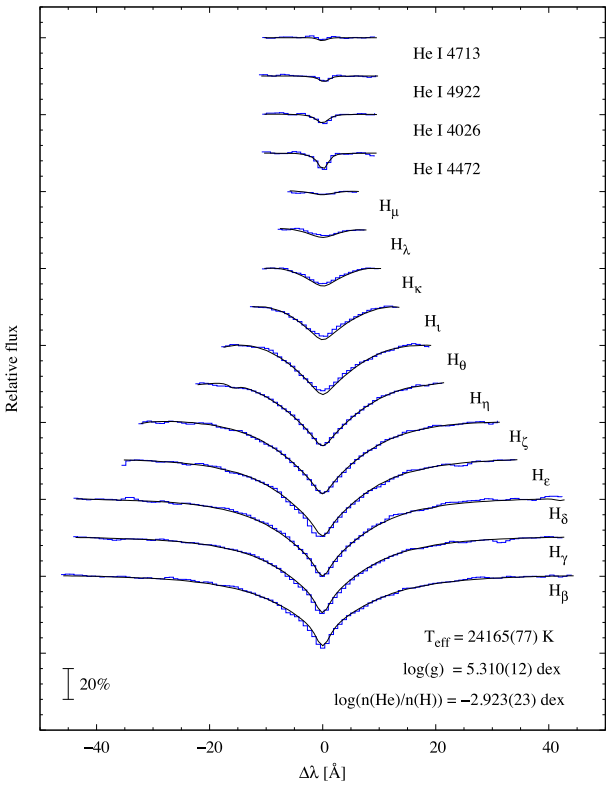

Figure 1. Spectra of KIC 2697388 obtained by the WHT.

[1] http://archive.stsci.edu/kepler/

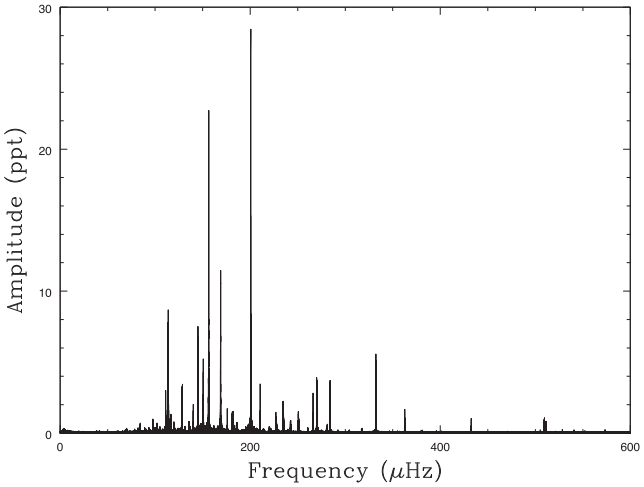

Figure 2. FT of the g-mode region.

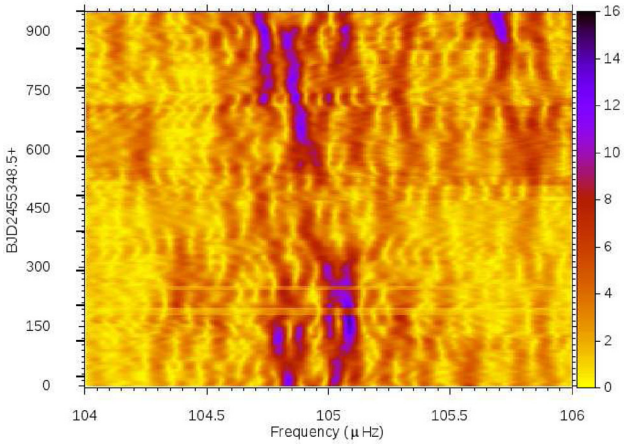

Figure 3. sFT showing varying periodicities at 105 μHz. Each line of the sFT is a separate FT which spans 200 d, and the ordinate indicates the mid-point of the data. Thick lines on the ordinate indicate where quarters change. Colour indicates amplitude in standard deviations with a scale bar to the right.

for indications that the periodicities are artefacts (e.g. frequency variations which match those of known spacecraft artefacts).

We then fitted the full-length FT with a Lorentzian profile to extract pulsation frequencies and amplitudes for peaks which exceeded detection limits in several FTs. The Lorentzian widths are used as an estimate of the error in frequency, which is often caused by amplitude and/or frequency variations over the span of the data. As shown by the sFT in Fig. 3, the amplitudes and frequencies of many multiplets vary over the course of three years, which, in turn, increases uncertainties in periodicities determined from the full data set. In total, we fitted 253 significant frequencies in which all but 23 were in the g-mode pulsation region below 1000 μHz. The highest amplitude periodicities and most complete period sequences are from 65 to 400 μHz, where 190 frequencies are located. Table 1 provides a sample list of KIC 2697388 's seismic properties, with the full list provided as on-line material.

3.1 The p-mode region

There are two groups of periodicities in the p-mode region near 2880 and 3800 μHz, each consisting of several, complex, amplitude- and/or frequency-varying periodicities. For these regions, the complete *Kepler* data set is crucial as the pulsations appear to be short-lived, with some similarity to KIC 2991276 (Østensen et al. 2014) but with increased complexity. The two more complex regions are shown in Fig. 4. Using the individual FT members of the sFTs, we fitted 23 p-mode frequencies. As these regions are extremely complex, we have chosen to be cautiously liberal in extracting frequencies – if the amplitude exceeded 4σ in any of the 200 d FTs which constitute the sFTs, we likely fitted it. We attempted to avoid regions where pulsations appear to merge or interact with one another, fitting as many frequencies from an individual FT as was possible. For this reason, some of the S/N values listed in Table 1 are <4, even though at some point the frequency exceeded that value. Examples are shown in the bottom panels of Fig. 4. The two major groupings near 2880 and 3800 μHz are separated by about 900 μHz, which is consistent with consecutive p-mode overtones listed in models (Charpinet et al. 2011). These frequencies will be discussed further in Section 3.5.

3.2 Period spacing

While Baran (2012) already found the asymptotic period spacing sequence for KIC 2697388, we repeated the exercise, without bias from their results, and using our expanded period list, to confirm those results and identify more periodicities. We used five $\ell = 1$ candidate multiplets (triplets or doublets) as the foundation for the $\ell = 1$ period spacing sequence. Similarly, we found five quintuplets and used them as the starting point for the $\ell = 2$ period spacing sequence. As in previous papers (e.g. Reed et al. 2011), we also produced a Kolmogorov–Smirnov (KS) test for reference. The KS test for KIC 2697388 (shown in Fig. 5) revealed the most significant period spacing near 140 s, its overtone near 70 s, and then a spacing near 240 s. Next, we iteratively found the period-spacing sequences by computing a linear regression fit, calculating a model sequence based on the fit, searching for additional periods near to the model ones, and updating the fit. Using this process, we determined that 56 periodicities fit the $\ell = 1$ period spacing sequence, 76 periodicities fit the $\ell = 2$ sequence, and 28 fit both. Our final linear regression fit produced an $\ell = 1$ sequence of 240.06 ± 0.19 s and an $\ell = 2$ sequence of 138.83 ± 0.35 s, essentially in exact agreement with Baran (2012).

Another tool for visualizing period sequences are echelle diagrams. These plot periods versus modulo of the period spacings so periods which fall on sequences line up vertically on the diagram. The portions of the echelle diagrams where there are nearly consecutive overtones are shown in Fig. 6. The $\ell = 2$ sequence (left-hand panel) stays very close to the asymptote, while the $\ell = 1$ sequence (right-hand panel) meanders about the asymptotic value. This behaviour has been previously noticed (Baran & Winans 2012) and will be discussed in Section 4. Each sequence also has some points away from the sequence, which is indicative of mode trapping.

3.3 Mode trapping

Mode trapping, where abrupt composition changes within the star disrupt asymptotic period spacings, has been detected in two other sdBV stars (Østensen et al. 2014; Foster et al. 2015) and so we search for them too. KIC 2697388 has a multiplet with $\ell = 2$ like splittings, which does not fit the asymptotic period spacing sequence (see Fig. 6). This could be a trapped mode, and so we produced a reduced period diagram, which plots reduced periods,

Table 1. KIC 2687388's periodicities and associated mode identifications. Errors are provided in parentheses. Column 5 provides the data set in which the frequency was fitted. Data sets starting with Q span three quarters from the stated quarter, those starting with D span 200 d from the stated start day, and All represents the entire data set. Column 6 provides our mode identifications and Column 7 those from Reed et al. (2011)† with both using n as the radial index from asymptotic relations. Column 8 provides mode identifications from two models (tables 3 and 4 of Charpinet et al. 2011)⋆, where the radial index k is from those models. Column 9 lists mode identifications from Baran (2012)◇, for which no radial indices were published. A '–' in columns 6–9 indicates that the periodicity was detected, but the index was not assigned. Column 10 provides deviations from our asymptotic period spacings, and column 11 lists frequency multiplet splittings.

ID	Frequency (μHz)	Period (s)	S/N	Set	Mode (us) ℓ, m, n	Mode† ℓ, n	Mode⋆ ℓ, k Model 1/Model 2	Mode◇ ℓ, m	$\frac{\Delta P}{\Delta \Pi}$ (per cent)	$\Delta\nu$ (μHz)
f084	275.105 (0.022)	3634.976 (0.291)	5.2	Q14						
f085	270.851 (0.026)	3692.067 (0.354)	98.6	Q06	2, 2, 27		–	2, 2	−6.6	0.233
f086	270.618 (0.050)	3695.246 (0.683)	65.3	Q06	2, 1, 27			2, 1	−4.7	0.200
f087	270.418 (0.058)	3697.979 (0.793)	27.1	Q06	2, 0, 27	2, 24	2,−27/2,−27		−2.8	0.228
f088	270.190 (0.026)	3701.099 (0.356)	84.3	Q06	2, −1, 27		–	2, −1	−0.6	0.204
f089	269.986 (0.029)	3703.896 (0.398)	67.9	Q06	2, −2, 27			2, −2	1.3	
f090	266.164 (0.028)	3757.082 (0.395)	51.5	Q07	1, –, 16	1, 14	1, −15/1,−15	1, –	−2.5	
f091	261.267 (0.041)	3827.502 (0.601)	5.1	Q05	2, 2, 28			2, 2	−8.7	0.242
f092	261.025 (0.053)	3831.051 (0.778)	5.2	Q05	2, 1, 28			2, 1	−6.5	0.249
f093	260.776 (0.030)	3834.709 (0.441)	4.5	Q05	2, 0, 28				−4.2	0.178
f094	260.598 (0.044)	3837.328 (0.648)	6.3	Q05	2, −1, 28			2, -1	−2.3	0.198
f095	260.400 (0.071)	3840.246 (1.047)	6.7	Q05	2, −2, 28				−0.4	
f096	251.397 (0.026)	3977.772 (0.411)	25.4	Q08	2, 2, 29			2, 2	−1.3	0.180
f097	251.217 (0.043)	3980.622 (0.681)	31.4	Q06	2, 1, 29	1, 15/2, 26	2,−29/1,−16		0.8	0.225
f098	250.992 (0.028)	3984.191 (0.444)	30.7	Q06	2, 0, 29				3.4	0.246
f099	250.746 (0.025)	3988.100 (0.398)	65.4	Q14	2, −1, 29		–	2, −1	6.2	0.124
f100	250.622 (0.022)	3990.073 (0.350)	23.1	Q06	2, −2, 29			2, −2	7.6	

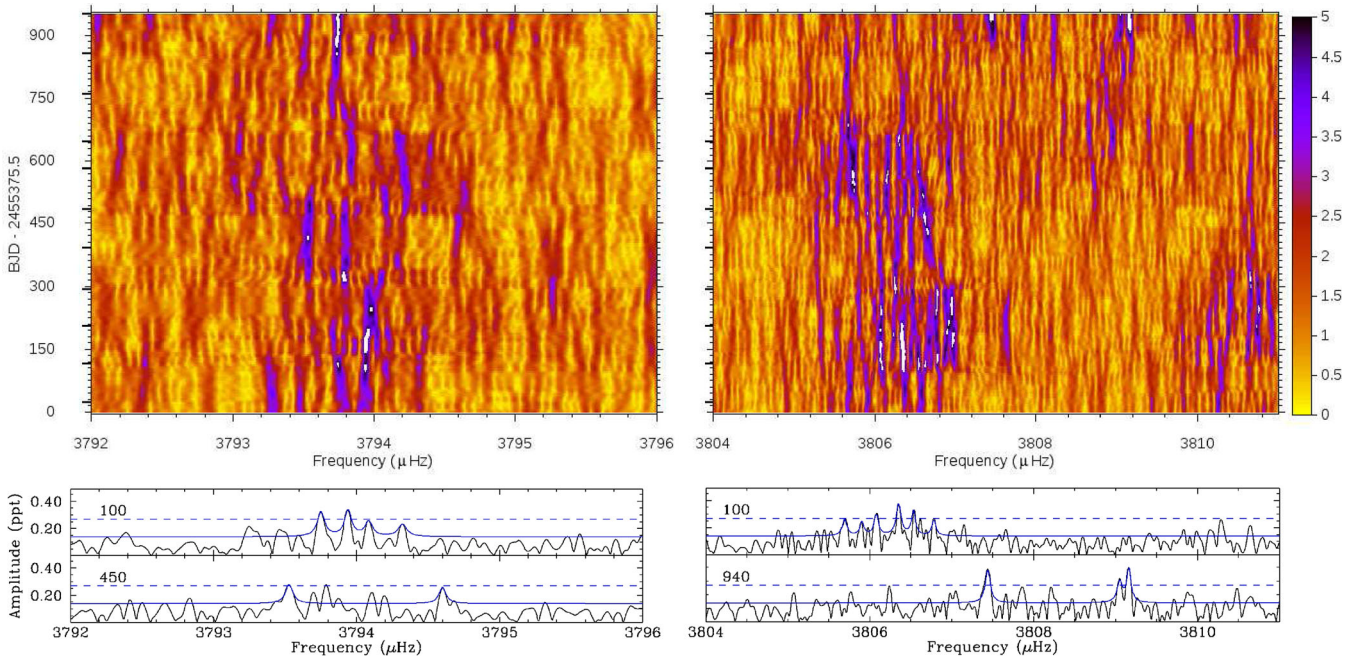

Figure 4. sFTs (top panels) shown with select individual FTs (bottom panels). White patches within the sFTs indicate amplitudes $>5\sigma$. Bottom panels: individual FTs which make up the sFTs, with the corresponding day indicated in each panel. Horizontal (blue) lines indicate a 4σ detection limit with Lorentzian fits shown as solid (blue) lines. These FTs are examples and do not necessarily indicate the FT used for the values provided in Table 1.

$\Pi = P\sqrt{\ell(\ell+1)}$, against reduced period spacings. This makes the periods degree-independent and, since all modes of the same radial order should be trapped, they should line up in the diagram.

Fig. 7 shows the reduced period plot for $n = 21$–45. Both $\ell = 1$ and 2 pulsations have complete sequences between $n = 21$ and 32 except for one missing mode at n, $\ell = 22$, 1. As expected, the $\ell = 2$ multiplet described above appears as a trapped mode at $\Pi_2 = 10$, 217 s between $n = 30$ and 31. There should be a corresponding $\ell = 1$ mode, and we find a periodicity at $\Pi_1 = 10\,293$ s, which also fits the $\ell = 2$ asymptotic sequence ($P = 7278.762$ s). Based on multiplet structure, we interpret this periodicity as the corresponding trapped $\ell = 1$ mode. It appears that KIC 2697388 is the third sdB variable to show a trapped mode. Like the other two, it is an outlier in an otherwise complete sequence.

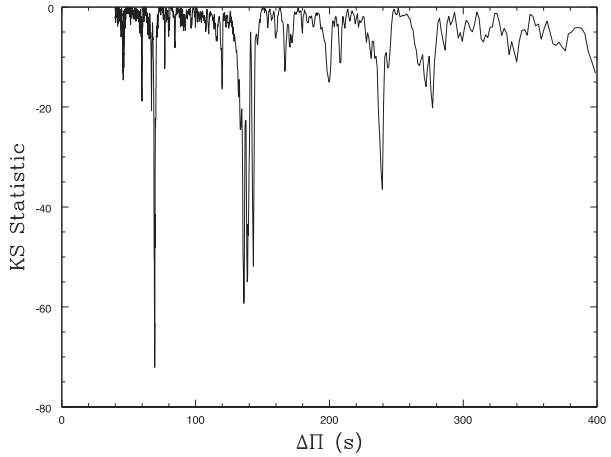

Figure 5. KS test of KIC 2697388.

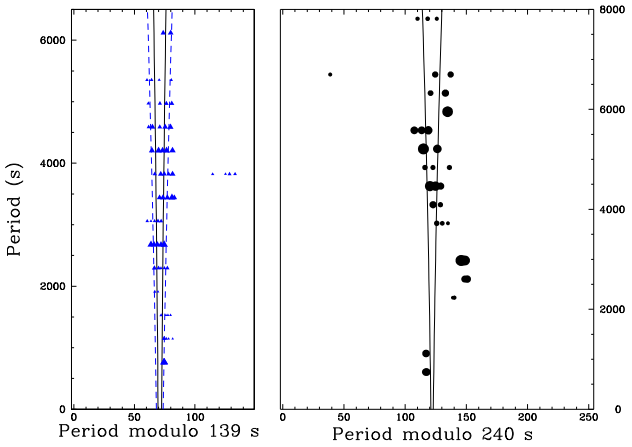

Figure 6. Echelle diagrams by mode. Blue triangles indicate $\ell = 2$ pulsations, while black circles indicate $\ell = 1$.

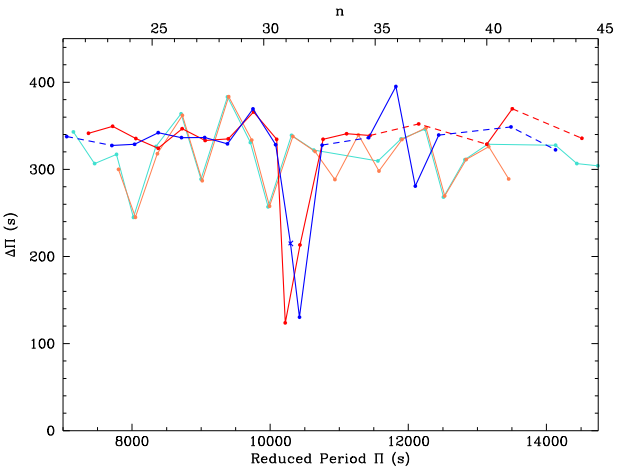

Figure 7. Reduced period diagram. Solid points represent pulsations identified originally by period spacing and/or frequency splittings. Blue lines/points indicate $\ell = 1$ and red lines/points indicate $\ell = 2$ with lighter versions for the model from Charpinet et al. (2011). The cross-point indicates the trapped $\ell = 1$ pulsation, which also fits the $\ell = 2$ period spacing sequence. Solid lines indicate consecutive overtones, while dashed lines indicate missing overtones.

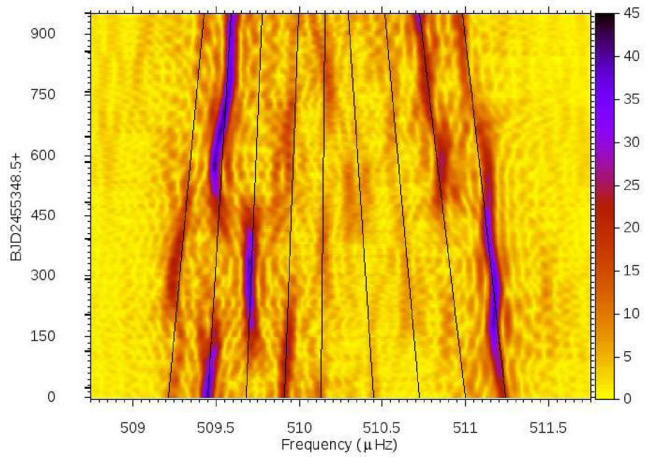

Figure 8. Example of a convergent $\ell = 4$ multiplet at ∼510 μHz. Lines are for guidance only, to indicate temporal evolution of each m value.

3.4 High-degree modes

Using our $\ell = 1$ asymptotic sequence, we generated model period sequences for $\ell = 3$ and 4. Since the spacing between overtones decreases with increasing degree, we cautiously searched for periods to fit these sequences, requiring them to have multiplets with too many members to be $\ell = 2$. Four multiplets show characteristics associated with $\ell \geq 3$ and occur at ∼181, ∼185, ∼510, and 891 μHz. Most prominent are the seven periodicities centred at ∼510 μHz having multiplet structure associated with $\ell = 4$, the sFT of which is shown in Fig. 8. Two sets of multiplets at ∼181 and ∼185 μHz are within 10 per cent of the $\ell = 4$ sequence and were identified as such. Therefore, using period spacings and frequency splittings, we found 24 $\ell = 4$ modes.

3.5 Frequency splittings

Frequency multiplets occur when azimuthal degeneracy is lifted, usually by rotation. As noted in Baran (2012), KIC 2697388 has many sets of clear frequency multiplets, and we found two common g-mode splittings near 0.14 and 0.22 μHz, many which also fell on the asymptotic sequences. We searched the rest of our frequencies for possible multiplets, and we were able to identify 48 frequencies as $\ell = 1$ with an average frequency splitting of 0.138 ± 0.013 μHz and 94 frequencies as $\ell = 2$ with an average splitting of 0.215 ± 0.017 μHz (during Q05–Q08, described below).

Interestingly, all full $\ell = 2$ quintuplets show convergence in their frequency splittings over the three years of observations. A similar feature was seen in the sdB p-mode pulsator Balloon 090100001 (Baran, Pigulski & O'Toole 2008, hereafter BA09), with two major differences: In BA09, the change in splitting was increasing, whereas it is decreasing in KIC 2697388, and whereas BA09 was observed during two runs obtained three years apart, ours is a continuous set. We fitted the frequencies early (quarters 5, 6, and 7, if possible) and late (quarters 14, 15, and 16, if possible) within the data for all multiplet members. As Table 2 shows, all $\ell = 2$ multiplets have convergences larger than their errors and at consistent rates. The individual $\ell = 1$ multiplets have rates near zero but with large errors which easily encompass the observed $\ell = 2$ rate. The degree-dependent value of the Ledoux constant means that $\ell = 1$ multiplets are 36 per cent closer together than $\ell = 2$ multiplets, and $\ell = 2$ multiplets have many more members (and we have more of them), making their splittings easier to determine. Fig. 9 shows

Table 2. Table of multiplets used to calculate convergence rates. Column 1 provides the mode, Columns 2 and 3 list the weighted average splittings early (typically quarters 5, 6, and 7, but always Q < 11) and late (typically quarters 14, 15, and 16, but always Q > 12) during the observations, and the last column provides the convergence rate. Averages for all of the $\ell = 1$ and 2 multiplets are provided on separate lines.

ℓ, n	Frequency (splitting early)	Frequency (splitting late)	$\Delta\nu/\Delta t$ (μHz yr^{-1})
1, 30	0.129 (0.029)	0.138 (0.030)	0.005 (0.041)
1, 28	0.133 (0.013)	0.108 (0.038)	− 0.014 (0.040)
1, 25	0.102 (0.037)	0.118 (0.036)	0.008 (0.056)
1, 21	0.129 (0.035)	0.134 (0.035)	0.005 (0.049)
Total convergence rate of $\ell = 1$			− 0.0006 (0.0226)
2, 31	0.231 (0.006)	0.182 (0.006)	− 0.024 (0.008)
2, 30	0.218 (0.007)	0.159 (0.006)	− 0.029 (0.009)
2, 28	0.219 (0.010)	0.165 (0.007)	− 0.036 (0.012)
2, 27	0.216 (0.006)	0.180 (0.007)	− 0.021 (0.010)
2, 26	0.215 (0.003)	0.180 (0.007)	− 0.020 (0.008)
Total convergence rate of $\ell = 2$			− 0.0249 (0.0041)
4, 15	0.275 (0.036)	0.226 (0.029)	− 0.025 (0.046)
4, 26	0.237 (0.003)	0.203 (0.003)	− 0.019 (0.004)
4, 72	0.227 (0.021)	0.191 (0.008)	− 0.021 (0.022)
4, 74	0.251 (0.007)	0.178 (0.028)	− 0.042 (0.029)
Total convergence rate of $\ell = 4$			− 0.0195 (0.0039)

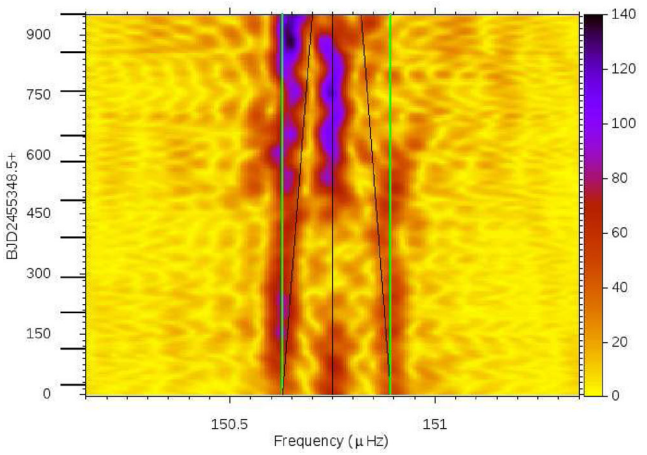

Figure 9. Same as Fig. 8, for an example of an $\ell = 1$ triplet at ∼150 μHz with black lines showing the $\ell = 2$ convergence rate and green lines the constant frequency.

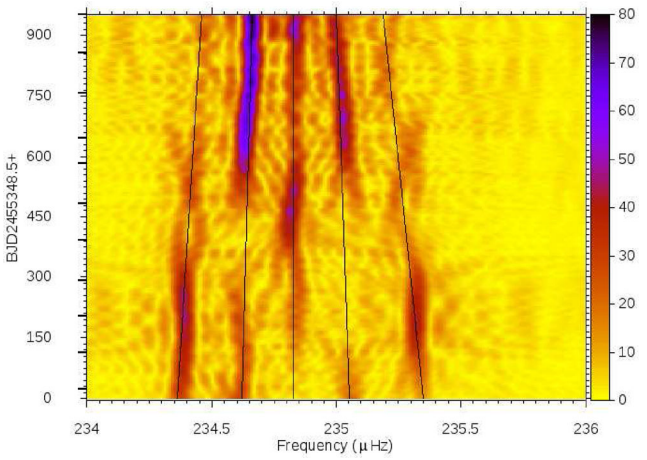

Figure 10. Same as Fig. 8, for an example of a convergent $\ell = 2$ quintuplet at ∼235 μHz.

the only converging $\ell = 1$ multiplet, with lines for both the $\ell = 2$ convergence rate and constant frequency. It can be seen that the frequencies do narrow slightly but remain closer to constant. For comparison, Fig. 10 shows an $\ell = 2$ converging multiplet. The result is that we can readily determine that $\ell = 2$ splittings are converging at a uniform rate, but the four $\ell = 1$ multiplets individually have errors both consistent with zero and the rate observed for $\ell \geq 2$ multiplets. Ensemble analysis of both sets results in our reported value for $\ell = 2$ of -0.0249 ± 0.0041 μHz yr^{-1} and a slightly negative value for $\ell = 1$, which is consistent with zero and within 1σ of our $\ell = 2$ rate. We cannot rule out that all modes are converging at the same rate, though it is most likely that the $\ell = 1$ modes are not converging.

This convergence is also observed in $\ell = 4$ multiplets. The best example is the $n = 26$ multiplet centred at ∼510 μHz with a convergence rate of -0.019 ± 0.004 μHz yr^{-1}. The multiplet has missing components between 510.160 and 510.900 μHz, but using the remaining multiplet members, it is reasonable to allow for these two missing components. Including these, the multiplet has nine components and an average frequency splitting of 0.243 ± 0.050 μHz in Q06– Q08. Values for ℓ and m are assigned with respect to this evidence. Three other $\ell = 4$ multiplets have at least two members which appear both near the beginning and near the ending of the data set, which could be used to determine a convergence rate. The errors are much larger than for the $n = 26$ multiplet, but the rate is similar. The weighted average of the $\ell = 4$ multiplets is dominated by the $n = 26$ multiplet and is -0.0195 ± 0.0039. Table 2 lists all the multiplets used in the convergence rate calculations. If this convergence continues, multiplets would become singlets in only ∼9 yr.

In the p-mode region, there are two frequencies near 2868 μHz and two near 2908 μHz, which are sufficiently constant to be easily separable. Around 3793 and 3807 μHz, the multiplets are both richer and more variable. A total of 7 frequencies were fitted near the former and 12 near the latter. The average frequency splitting (divided by Δm for splittings of $\Delta m > 1$) near 3793 is 0.219 ± 0.047, which is similar to the average of the splittings between f001 and f012 of the 3806 group, which is 0.218 ± 0.044. The two splittings of the 2880-μHz groups are dissimilar, and so cannot

be used for mode identification. They could be low-degree modes, but the ones near 3800 μHz must have $\ell \geq 3$. If all the frequencies near 3808 μHz belong to the same multiplet, then it would require $\ell \geq 12$, which seems unlikely. f001–f003 forms a triplet and f007–f012 is an $\ell = 3$ multiplet with no missing members, so these are the most likely identifications. However, there are other splittings in this group which are near-integer multiples of 0.21 μHz, so we cannot rule out that this complex is a single high-degree mode. Since the groups near 3793 and 3806 μHz are too close together to be consecutive overtones, f007–f012 and f013–f019 cannot both be $\ell = 3$. For this reason, in Table 1, we list them both as $\ell \geq 3$.

3.6 Rotation period

As is standard practice, we assume that rotation is lifting the azimuthal degeneracy of the multiplets, allowing us to calculate the rotation period of KIC 2697388, as in our previous papers (e.g. Baran et al. 2012; Telting et al. 2012; Reed et al. 2014). From the $\ell = 1$ multiplets, with a Ledoux constant of 0.5, we derive the rotational period to be 41.94 ± 3.61 d. Due to the convergence in all $\ell \geq 2$ multiplets, the derived rotation period is time-dependent. We note that the $\ell \geq 2$ splittings are consistent in relation to the $\ell = 1$ splittings early during the campaign and so again use data from the first year of *Kepler* observations. Using a Ledoux constant of 0.166 for $\ell = 2$ modes and frequency splittings of 0.215 ± 0.017 μHz in Q05–Q08, the rotational period is 44.86 ± 6 d. Likewise, using a Ledoux constant of 0.05 for $\ell = 4$ and frequency splittings of 0.243 ± 0.050 μHz in Q06–Q08, the rotational period is 45.21 ± 7 d. These calculations are self-consistent, and we suggest a rotation period for KIC 2697388 of nearly 42 d. This period is consistent with, but slightly smaller than, that determined by Baran (2012) of 45 d. We suspect that the wider $\ell = 2$ and 4 multiplets at the beginning of *Kepler's* observations influenced the Baran (2012) value. Note that even though the $\ell = 2$ and 4 frequency splittings decrease with time, their ratio remains at 0.885 ± 0.031, which is consistent with the theoretical value of 0.877.

While not as clearly defined, the p-mode multiplets also are consistent with the g-mode results, consistent with solid-body rotation for KIC 2697388. The separations of the two extensive multiplets (f001–f019), using $C_{n,\ell} = 0$, is 53 ± 9 d. A small Ledoux constant would make this value even closer to the g-mode one. As such, it would seem that KIC 2697388 rotates uniformly like KIC 10139564 and not differentially like KIC 3527751.

4 SUMMARY AND DISCUSSION

From our 21 low-resolution spectra obtained using the NOT and WHT, and after applying standard reduction steps, we could not find any significant periodic RV signal. Although RV measurements show noticeable scatter with rms = 9.5 km s^{-1}, the RV data are consistent with KIC 2697388 being a single star. However, further accuracy is needed to sufficiently rule out binarity.

From the complete *Kepler* SC data set covering Q05–Q17, we detected 253 periodicities. The vast majority of these have periods between 1 and 2.5 h, which we associated with g-mode pulsations. KIC 2697388 also has 23 periodicities located in the p-mode region (1000–8494 μHz), with multiplets detected among them.

Asymptotic period spacings were found in the low-frequency region. In agreement with previous results (Baran 2012), period spacings for $\ell = 1$ and 2 pulsation modes are 240.06 ± 0.19 and 138.83 ± 0.35 s. We measure the ratio between $\ell = 1$ and 2 period spacings to be 1.73 ± 0.16, which agrees with the slow rotation asymptotic theory value of $\sqrt{3}$ (Ledoux 1951). The p-mode pulsations are separated by roughly 900 μHz, which is consistent with models (Charpinet et al. 2002), but inconsistent with the previous *Kepler* observed p-mode pulsator KIC 10139564, which has overtone values near 200 s (Baran et al. 2012). However, since we cannot identify the p- modes, and there are so few of them, our results are far less robust than for KIC 10139564.

A model was calculated for KIC 2697388 by Charpinet et al. (2011) using their third-generation (3G) model grid and fitted to the *survey -phase* data which consisted of only one month of observations. They used their forward method of matching model to observed frequencies without observational constraints on mode degrees, as none were available at that time. Under those conditions, they found two model solutions which matched the observed frequencies and spectroscopic limits and provided very reasonable physical properties for the star. With observational mode identifications, we find their identification accuracy to be 55 per cent for both models 1 and 2. In the reduced period diagram (Fig. 7), we have included their model 1 solution (model 2 does not differ significantly) plotted with the observed reduced periods. The model 1 (2) reduced period spacing is 315 ± 34 (318 ± 32), while our observed one is 339 ± 18 s. The spacing itself is a reasonable match, but the scatter between individual periods is double, averaging to 46.5 s in the model and 21.4 s from the observations. There is no direct way to interpret these differences. First, we do not know how their model would match when observational-mode constraints are used. And perhaps most importantly, their models have undergone updates since their publication (e.g. Charpinet et al. 2014). The useful takeaway from our reduced period comparison is the period-to-period deviation of the period spacings. It has been shown that diffusion can smooth the core–envelope transition (Hu et al. 2009; Miller Bertolami, Córsico & Althaus 2012), which reduces the theoretical period spacing spread and more closely matches the observations. We eagerly await comparisons with updated models.

While models originally predicted large amounts of mode trapping (e.g. Charpinet et al. 2002), one or two trapped modes in an otherwise smooth asymptotic sequence have now been detected in three stars (this work; Østensen et al. 2014; Foster et al. 2015). Miller Bertolami et al. (2012) produced a similar feature (bottom right-hand panel of their fig. 2) by including overshoot at the He-burning core. However, this overshoot increases the chemical complexity of the boundary layer, with the result that even period spacings are disrupted much more than is observed. Overshoot may point to the cause of mode trapping, but a thorough comparison with the precision asteroseismology revealed by *Kepler* has yet to be accomplished for any sdBV star.

Regular frequency splittings were found for multiplets of the same ℓ degree, including some multiplets with too many members to be $\ell \leq 2$, which we identified as $\ell = 4$. The average frequency splittings for $\ell = 1$ multiplets are 0.138 ± 0.013, for $\ell = 2$ multiplets, 0.215 ± 0.017 μHz in Q05–Q08, and for $\ell = 4$ multiplets, 0.243 ± 0.050 μHz in Q06—Q08. The frequency splittings for $\ell \geq 2$ converge throughout the observations, and the splittings of $\ell = 2$ and 4 converge consistently with each other. From the $\ell = 1$ frequency splittings, we derive a rotational period of ∼42 d, which is slightly smaller than that found by Baran (2012).

Whenever possible, we used both asymptotic period spacing and frequency splittings to identify 224 periodicities (89 per cent) with modes varying from $\ell = 1$ to 4. Fig. 11 is an amplitude-weighted echelle diagram showing our mode identifications for all of KIC 2697388's pulsations (which also appear in Table 1).

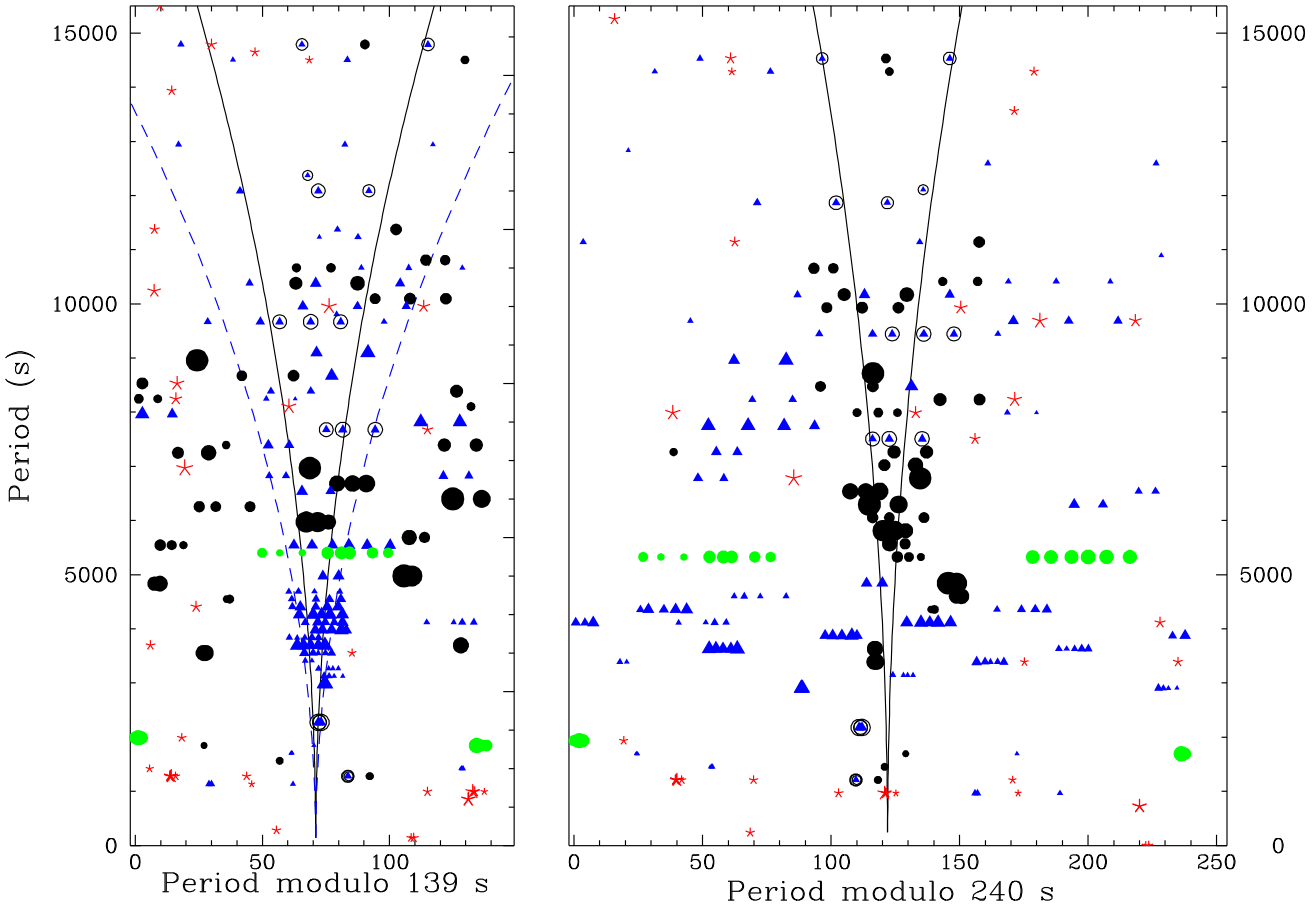

Figure 11. Echelle diagram like Fig. 5 but including all pulsations for KIC 2697388. The points are amplitude weighted so largest points represent the highest amplitude pulsations. Modes are indicated by black circles for $\ell = 1$, blue triangles for $\ell = 2$, green circles for $\ell = 4$, and red asterisks for unidentified modes. Modes which could be either $\ell = 1$ or 2 appear as blue triangles surrounded by black circles. The diverging vertical lines indicate multiplet frequency splittings.

Certainly our most interesting result is the converging frequency splittings seen in $\ell \geq 2$ modes. Those multiplets are converging at a rate of $-0.024\,86 \pm 0.000\,02\ \mu\mathrm{Hz\ yr^{-1}}$ (a change in rotation period of $-4.7\ \mathrm{dyr^{-1}}$), which would convert multiplets to singlets in the course of only about nine years. The $\ell \geq 4$ convergence is consistent with the $\ell \geq 2$ rate, while the $\ell \geq 1$ multiplets are the most consistent with *no change* but overlap the rate seen in the $\ell \geq 2$ multiplets at the 1σ level. It would seem unphysical to associate this phenomenon with the rotation of the star as a whole when one considers the following: (i) We do not know of any mechanism which could apply sufficient torque to completely stop stellar rotation within a decade. (ii) It would be implausibly fortuitous that we observe this star during the decade when its spin goes from observable to zero.

An explanation for changes in multiplets of the sdBV star BA09 was posited by Pérez, Oreiro & Hu (2011), who modelled an exchange of angular momentum between rotation and pulsations. This effect would locally change rotation, establishing differential rotation (see equation 2 of Pérez et al. 2011) with g-mode pulsations driving changes in p-mode multiplets (via changes in near-surface rotation). A consequence of this coupling is that g-mode amplitudes should change in correspondence with energy exchanged between pulsations and rotation, and we do not observe any such correlation for KIC 2697388. Of course, those amplitude variations could be masked by amplitude variations from other intrinsic causes, as we see them in nearly every sdBV star. Likewise, we do not observe any indications of differential rotation, though again our evidence is not substantial as the p-mode multiplets have amplitudes which are not long-lived during these observations. And finally, this mechanism should preferentially be changing p-mode multiplets, whereas we observe changes in the g-mode splittings. KIC 2697388 should be a good test case for this mechanism, though we conclude that it is unlikely the cause of the observed multiplet changes for this star.

Another possibility is *resonant mode coupling*, as described by Zong et al. (2016) and Zong, Charpinet & Vauclair (2016) for a DB white dwarf and the sdBV star KIC 10139564. They describe three *regimes* of mode coupling, with only one effecting frequency. In that regime, they list the period of modulation as $P_{\mathrm{mod}} \approx 1/\delta\nu$, where $\delta\nu$ comes from Goupil, Dziembowski & Fontaine (1998) and $\delta\nu = 4C\Omega^2/\nu_o$ (equation 1 of Zong et al. 2016). Using appropriate numbers for KIC 2697388 would imply the shortest P_{mod} to be nearly 160 yr, which is far longer than what we observe. Zong et al. (2016) do include that the oscillations could have 'irregular, even chaostic [sic]' frequency modulations. Yet since all the $\ell = 2$ multiplets and the only $\ell = 4$ multiplet undergo the same change, it seems not to be chaotic. We are certainly interested to see if Zong et al. (2016) can fit the changes into their formalisms to explain the frequency convergence.

Another effect which could generate multiplets are magnetic fields. However, the field strength would need to be strong, and to date, only weak magnetic fields (or upper limits) have been measured for sdB stars (O'Toole et al. 2005).

While two ideas are known for evolving pulsation frequencies over short time-scales, neither truly satisfies the conditions of the converging multiplets observed in KIC 2697388. As such, we feel compelled to mention the disturbing prospect that multiplets in sdB stars might not be due to rotation at all but rather due to some as-yet-unknown mechanism. Since we have presumed the cause of multiplets to be rotation, and have used that to describe radially differential rotation (Foster et al. 2015) and subsynchronous rotation in close binaries (Pablo et al. 2012), those assertions would have to be re-evaluated, should another cause of multiplets be discovered.

The converging multiplets observed in KIC 3527751 are a very intriguing and challenging result, which heretofore had not been observed in sdBV stars. We still regard rotation as the most likely contributor for breaking azimuthal degeneracy which produces multiplets, though we hope our findings spark investigations for an explanation.

ACKNOWLEDGEMENTS

Funding for this research was provided by the National Science Foundation grant#1312869. Any opinions, findings, and conclusions or recommendations expressed in this material are those of the author(s) and do not necessarily reflect the views of the National Science Foundation. JWK was partially supported by the Missouri Space Grant Consortium, funded by NASA. ASB gratefully acknowledges a financial support from the Polish National Science Center under project No. UMO-2011/03/D/ST9/01914. This paper includes data collected by the *Kepler* mission. Funding for the *Kepler* mission is provided by the NASA Science Mission directorate. Data presented in this paper were obtained from the Mikulski Archive for Space Telescopes (MAST). STScI is operated by the Association of Universities for Research in Astronomy, Inc., under NASA contract NAS5-26555. Support for MAST for non-*HST* data is provided by the NASA Office of Space Science via grant NNX13AC07G and by other grants and contracts.

REFERENCES

Baran A. S., 2012, Acta Astron., 62, 179
Baran A. S., Winans A., 2012, Acta Astron., 62, 343
Baran A., Pigulski A., O'Toole S. J., 2008, MNRAS, 385, 255 (BA09)
Baran A. S. et al., 2012, MNRAS, 424, 2686
Baran A. S., Telting J. H., Nemeth P., Bachulski S., Krzesinski J., 2015, A&A, 573, A52
Baran A. S., Telting J. H., Nemeth P., Østensen R. H., Reed M. D., Kiaeerad F., 2016, A&A, 585, A66
Charpinet S., Fontaine G., Brassard P., Dorman B., 2002, ApJS, 139, 487
Charpinet S. et al., 2011, A&A, 530, A3
Charpinet S., Brassard P., van Grootel V., Fontaine G., 2014, in van Grootel V., Green E., Fontaine G., Charpinet S., eds, ASP Conf. Ser. Vol. 481, On Interpreting g-Mode Period Spacings in sdB Stars. Astron. Soc. Pac., San Francisco, p. 179
Edelmann H., Heber U., Hagen H.-J., Lemke M., Dreizler S., Napiwotzki R., Engels D., 2003, A&A, 400, 939
Foster H. M., Reed M. D., Telting J. H., Østensen R. H., Baran A. S., 2015, ApJ, 805, 94
Goupil M. J., Dziembowski W. A., Fontaine G., 1998, Balt. Astron., 7, 21
Heber U., Hunger K., Jonas G., Kudritzki R. P., 1984, A&A, 130, 119
Heber U., Reid I. N., Werner K., 2000, A&A, 363, 198
Hu H., Nelemans G., Aerts C., Dupret M., 2009, A&A, 508, 869
Ledoux P., 1951, ApJ, 114, 373
Miller Bertolami M. M., Córsico A. H., Althaus L. G., 2012, in Kilkenny D., Jeffery C. S., Koen C., eds, ASP Conf. Ser. Vol. 452, Exploring the Effects of Detailed Chemical Profiles on the Adiabatic Oscillation Spectrum of sdB Stars: First Results. Astron. Soc. Pac., San Francisco, p. 175
O'Toole S. J., Jordan S., Friedrich S., Heber U., 2005, A&A, 437, 227
Pablo H. et al., 2012, MNRAS, 422, 1343
Pérez F., Oreiro R., Hu H., 2011, A&A, 535, A96
Reed M., Foster H., 2014, in van Grootel V., Green E., Fontaine G., Charpinet S., eds, ASP Conf. Ser. Vol. 481, Precision Observational Asteroseismology Using Kepler Spacecraft Data. Astron. Soc. Pac., San Francisco, p. 45
Reed M. D. et al., 2010, MNRAS, 409, 1496
Reed M. D. et al., 2011, MNRAS, 414, 2885
Reed M. D., Foster H., Telting J. H., Østensen R. H., Farris L. H., Oreiro R., Baran A. S., 2014, MNRAS, 440, 3809
Saffer R. A., Bergeron P., Koester D., Liebert J., 1994, ApJ, 432, 351
Telting J. H. et al., 2012, A&A, 544, A1
Telting J. H. et al., 2014, A&A, 570, A129
Zong W., Charpinet S., Vauclair G., Giammichele N., Van Grootel V., 2016, A&A, 585, A22
Zong W., Charpinet S., Vauclair G., 2016, A&A, 594, 46
Østensen R. H. et al., 2010, MNRAS, 409, 1470
Østensen R. H., 2010, Astron. Nachr., 331, 1026
Østensen R. H. et al., 2010, MNRAS, 408, L51
Østensen R. H. et al., 2011, MNRAS, 414, 2860
Østensen R. H., Telting J. H., Reed M. D., Baran A. S., Nemeth P., Kiaeerad F., 2014, A&A, 569, A15
Østensen R. H., Reed M. D., Baran A. S., Telting J. H., 2014, A&A, 564, L14

SUPPORTING INFORMATION

Supplementary data are available at *MNRASJ* online.

on-line_table

Please note: Oxford University Press is not responsible for the content or functionality of any supporting materials supplied by the authors. Any queries (other than missing material) should be directed to the corresponding author for the article.

This paper has been typeset from a TEX/LATEX file prepared by the author.